Revue des Energies Renouvelables Vol. 12 N°2 (2009) 279 – 297

Modeling of polycrystalline N^+/P junction solar cell with columnar cylindrical grain

A. Trabelsi*, A. Zouari and A. Ben Arab

Laboratoire de Physique Appliquée, Département de Physique
Faculté de Sciences, Université de Sfax, B.P. 1171, Sfax, Tunisie

Abstract - *Analytical expressions for short-circuit and dark current densities are derived for a polycrystalline N^+/P junction solar cell. A new solution of the continuity equation for the minority carrier which is adaptable with the boundary conditions when the cell is either illuminated or in the obscurity is given. For the first time, a three-dimensional model is developed for a polysilicon solar cell with multi-cylindrical grains. For an elementary solar cell, the results show that the three types of recombination such as the bulk recombination, the surface recombination and the recombination at the grain boundaries have an important effect on the cell parameters; and in some cases, one of these forms of recombination dominates the others. In the case of multi-cylindrical grains, the results of our approach show a decrease of the photovoltaic parameters according to the grain number especially for a thick solar cell. In addition, the comparison between an elementary cylindrical grain solar cell and an elementary cubic grain one shows an enhancement of the photovoltaic parameters for the cylindrical model.*

Résumé - *Des expressions analytiques pour la densité du courant de court-circuit et celle du courant d'obscurité sont présentées pour une cellule solaire élémentaire au silicium polycristallin. Une nouvelle solution de l'équation de continuité des porteurs minoritaires est donnée. Cette solution est adaptable avec les conditions aux limites de la cellule éclairée et à l'obscurité. Pour la première fois, un modèle tridimensionnel est développé pour une cellule solaire polycristalline avec plusieurs grains de géométrie cylindrique. Pour la cellule élémentaire, les résultats montrent que les trois types de recombinaison, à savoir: la recombinaison en volume, en surface et aux joints de grains ont un effet important sur les paramètres photovoltaïques de la cellule. Dans plusieurs cas, l'une des formes de recombinaison domine les autres. Dans le cas de la cellule à plusieurs grains cylindriques, les résultats de notre approche montrent une dégradation des propriétés photovoltaïques de la cellule par augmentation du nombre de grains surtout pour une cellule épaisse. De plus, la comparaison entre les modèles cubique et cylindrique a montré une légère amélioration des paramètres photovoltaïques en faveur du modèle cylindrique.*

Mots clés: Cellule solaire polycristalline – Grain cylindrique – Grain cubique – Joint de grain.

1. INTRODUCTION

Polycrystalline silicon is a very promising material for the production of inexpensive and efficient solar cells for the terrestrial photovoltaic applications [1]. However, polysilicon substrates suitable for such an application should have a columnar structure formed by the juxtaposition of silicon grains limited by the grain boundaries [1].

Moreover, the performance of polycrystalline solar cells is governed by many factors, among which are the intragrain material quality [2], the surface state [3] and the

* abdessalem_trabelsi@yahoo.fr

grain boundary properties [4]. In order to study the effects of some of these factors on the performance of polycrystalline solar cells, the continuity equation for excess minority carrier must be solved under the appropriate boundary conditions for the model used.

In most previous works [2-4], the performance of polysilicon solar cell is obtained from the analytical expressions for an equivalent single crystal cell having an effective lifetime and diffusion length. These expressions take into consideration the intragrain properties and the effect of the grain boundaries [5].

A number of authors presented solutions for the continuity equation for excess carrier density in polycrystalline cells using a two-dimensional model [6, 7]. Others presented a three-dimensional model [1, 8], but all of them considered a cubic geometry for the grain.

Kurobe *et al.* [9] used MEDICI (a commercial two dimensional semiconductor device simulator) for presenting the effect of the grain boundaries in polycrystalline silicon thin-film solar cells. They propose two kinds of models of Si grains.

One is a 'stripe structure' (cubic grain) applied for a zone melting recrystallisation (ZMR) film, and the other is a 'columnar structure' (cylindrical grain) applied for a film with preferential orientation to a foreign substrate deposited by plasma-enhanced CVD (PECVD) or a multicrystalline thin film.

Lanza *et al.* [10, 11] and Elnahwy *et al.* [12] developed a numerical model taking into account the three-dimensional nature of cylindrical grain. These authors presented a solution for the continuity equation for minority carrier which is adaptable only with the boundary conditions of an illuminated solar cell. So they were interested only in the photocurrent and the spectral response.

In this work, the three-dimensional continuity equation for the minority carrier is solved analytically for a cylindrical-grain model when the cell is either illuminated or in the obscurity. A new solution for this equation, adaptable with the boundary conditions, is then obtained.

The influence of the grain size, the recombination velocity at the back contact and at the grain boundaries on the photovoltaic solar cell parameters is studied. For the first time, this study presents analytical results in the case of a solar cell formed by $(n \times n)$ cylindrical grains. Moreover, the effect of the grain number on the solar cell parameters is also discussed.

2. THEORY

2.1 Elementary cell structure and model of calculation

We considered a polycrystalline N^+/P solar cell formed by cylindrical grains. The grains are assumed to have the same physical properties (doping concentration, minority carrier mobility and lifetime,.). The grain boundaries are considered to be perpendicular to the surface of the cell with a depth that equals the grain thickness, and characterized by a recombination velocity V_g. The emitter and the base doping profiles are considered to be uniform, so no field exists outside the space charge regions [6-8, 13]. The schematic structure for a single cylindrical grain of a polycrystalline N^+/P solar cell is shown in Figure 1.

Under these assumptions, the continuity equation for minority carrier generated by a monochromatic light is given as follows [12]:

$$\frac{\partial^2 \Delta m(r,z)}{\partial r^2} + \frac{\partial^2 \Delta m(r,z)}{\partial z^2} + \frac{1}{r}\frac{\partial \Delta m(r,z)}{\partial r} - \frac{\Delta m(r,z)}{L_m^2} = -\frac{g(z)}{D_m} \qquad (1)$$

where $\Delta m = \Delta n$ represents the generated excess electron density in the base region and $\Delta m = \Delta p$ represents the generated excess hole density in the emitter region.

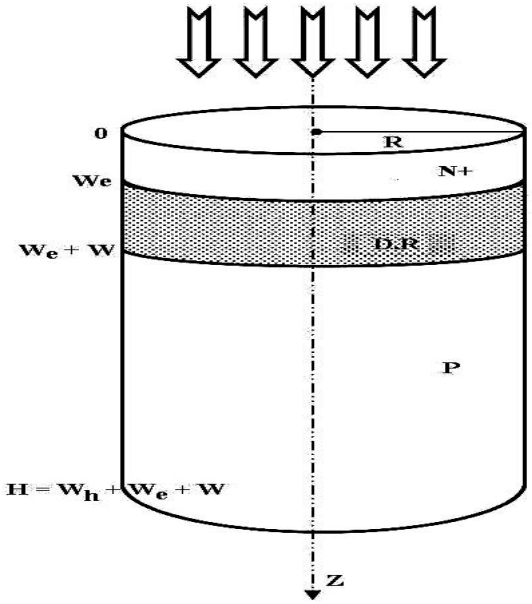

Fig. 1: Three-dimensional schematic model for an isolated columnar grain

The term $g(z)$ is the generation rate of minority carrier. In this study, we used the one presented by Mohammed [6]:

$$g(z) = \sum_{i=1}^{4} g_i . \exp(-\alpha_i z) \qquad (2)$$

α_i and g_i values are given in the **Table 1**.

Table 1: Coefficient of absorption of silicon α_i (cm^{-1}), g_i values ($cm^{-3}.s^{-1}$) correspond to AM_1 spectrum

α_1 = 633.079	α_2 = 102.664	α_3 = 14.7109	α_4 = 17805.8
$g_1 = 6.46746\times10^{19}$	$g_2 = 5.54674\times10^{18}$	$g_3 = 9.26415\times10^{17}$	$g_4 = 2.03553\times10^{21}$

2.1.1 Short-circuit current density in the base region

Referring to Figure 1, the boundary conditions in the base are:

- At the junction edge side of the base region, the excess electron density is under the short-circuit condition:

$$\Delta n(r,\ z = W_e + W) = 0 \tag{3}$$

- At the back contact, the surface is characterized by a recombination velocity S_n, so the excess electron density satisfies the following equation:

$$\left.\frac{\partial \Delta n}{\partial z}\right|_{z=H} = -\frac{S_n}{D_n}\Delta n(r, z = H) \tag{4}$$

- At the grain boundary, the excess minority carriers are governed by the grain boundary recombination velocity V_g and given by:

$$\left.\frac{\partial \Delta n}{\partial r}\right|_{r=R} = -\frac{V_g}{2D_n}\Delta n(r = R, z) \tag{5}$$

The continuity equation {Eq. (1)} allows a general solution given by:

$$\Delta n(r,z) = \sum_{i=1}^{4}\sum_{k\geq 0} f_{i,k}(r)\ \sin\left[C_k \times (z - W_e - W)\right] + K_1 \tag{6}$$

Using the {Eq. (3)} in {Eq. (6)}, we found K_1; so that the expression of the excess electron density becomes the same as given by [12].

The eigenvalues C_k which satisfy the boundary condition {Eq. (4)} are given by:

$$C_k\ \cot g(C_k.H) = -\frac{S_n}{D_n} \tag{7}$$

Using the {Eq. (6)} in the {Eq. (1)} and the {Eq. (5)}, the function $f_{i,k}(r)$ can be shown to have the form:

$$f_{i,k}(r) = A_{i,k}\, I_0\left(\frac{r}{Ln\, k}\right) + M_{i,k} \tag{8}$$

Where $$\frac{1}{L_{nk}^2} = \frac{1}{L_n^2} + C_k^2 \tag{9}$$

$$M_{i,k} = \frac{2g_i}{D_n}\frac{C_k^2\, L_{nk}^2}{C_k^2 + \alpha_i^2}\frac{\exp\left[-\alpha_i(W_e + W)\right]}{C_k W_b - \sin(C_k W_b)\cos(C_k W_b)}\left[1 + (-1)^{k+1}\exp(-\alpha_i W_b)\right] \tag{10}$$

$$A_{i,k} = -\frac{M_{i,k}}{I_0\left(\frac{R}{L_{nk}}\right) + \frac{2D_n}{V_g L_{nk}} I_0'\left(\frac{R}{L_{nk}}\right)} \tag{11}$$

$I_0(x)$ is the modified Bessel function of the first kind of zero order and $I_0'(x)$ is its first derivative with respect to its argument.

The photocurrent density, averaged over the cross section, at the junction edges in the base region, is given by:

$$J_{ph}^{B} = \frac{1}{\pi R^2} \int_0^R q D_n \left. \frac{\partial \Delta n(r,z)}{\partial z} \right|_{z=W_e+W} (2\pi r\, dr) \tag{12}$$

2.1.2 Short-circuit current density I_n the emitter region

Referring to the same Figure 1, the boundary conditions in the emitter are:

- At the junction edge side of the emitter region, the excess hole density is under the short-circuit condition:

$$\Delta p(r, z = W_e) = 0 \tag{13}$$

- At the top contact, the surface is characterized by a recombination velocity S_p, in such a way that the carrier density satisfies the following equation:

$$\left. \frac{\partial \Delta p}{\partial z} \right|_{z=0} = \frac{S_p}{D_p} \Delta p(r, z = 0) \tag{14}$$

- The equation (5) becomes for the emitter region:

$$\left. \frac{\partial \Delta p}{\partial r} \right|_{r=R} = -\frac{V_g}{2D_p} \Delta p(r = R, z) \tag{15}$$

- The continuity equation {Eq. (1)} allows a general solution given by:

$$\Delta p(r,z) = \sum_{i=1}^{4} \sum_{k \geq 0} f_{i,k}'(r) \sin\left[C'_k \times z\right] \tag{16}$$

The eigenvalues C_k' which satisfy the boundary condition {Eq. (14)} are given by:

$$C_k' \operatorname{cotg}(C_k' W_e) = \frac{S_p}{D_p} \tag{17}$$

The function $f_{i,k}'(r)$ can be shown to have the form:

$$f_{i,k}'(r) = B_{i,k} I_0\left(\frac{r}{L_{pk}}\right) + N_{i,k} \tag{18}$$

Where $$\frac{1}{L_{pk}^2} = \frac{1}{L_p^2} + C_k'^2 \tag{19}$$

$$N_{i,k} = \frac{2g_i}{D_n}\frac{C_k'^2 L_{pk}^2}{C_k'^2 + \alpha_i^2}\frac{1+(-1)^{k+1}\exp(-\alpha_i W_e)}{C_k' W_e - \sin(C_k' We)\cos(C_k' W_e)} \quad (20)$$

$$B_{i,k} = -\frac{N_{i,k}}{I_0(\,)() + \frac{2D_p}{V_g L_{pk}} I_0'(\frac{R}{L_{pk}})} \quad (21)$$

The photocurrent density, averaged over the cross section, at the junction edges in the emitter region, is given by:

$$J_{ph}^E = \frac{1}{\pi R^2}\int_0^R -q D_p \frac{\partial \Delta p(r,z)}{\partial z}\bigg|_{z=W_e} (2\pi r\, dr) \quad (22)$$

2.1.3 Short-circuit current density J_{ph}^R the depletion region

The short-circuit current J_{ph}^R in the depletion region, assuming that all carriers generated within this region are collected, is calculated by:

$$J_{ph}^R = \sum_{i=1}^{4} \frac{q g_i}{\alpha_i} \exp(-\alpha_i W_e).\left[1-\exp(-\alpha_i W)\right] \quad (23)$$

The photocurrent of the elementary solar cell is then obtained by adding up the above three contributions:

$$J_{ph} = J_{ph}^B + J_{ph}^E + J_{ph}^R \quad (24)$$

2.1.4 Dark current density in the base region

The dark minority carrier density in the base region satisfies the same continuity equation given by {Eq. (1)} but without the generation term.

The boundary conditions {Eq. (4)} and {Eq. (5)} used in the case of an illuminated cell are also valid under dark conditions. However, {Eq. (3)} has to be replaced by the Boltzmann condition [14]:

$$\Delta n(r, z = W_e + W) = \frac{n_i^2}{N_a}\left[\exp\left(\frac{V}{U_T}\right) - 1\right] \quad (25)$$

The expression of the excess minority carrier density $\Delta n(r,z)$ adaptable with the boundary condition given by {Eq. (25)} can be written as follows:

$$\Delta n(r,z) = \sum_{k\geq 0} h_k(r)\,\sin\left[C_k \times (z - W_e - W)\right] + K_3 \quad (26)$$

K_3 was given by the boundary condition {Eq. (25)}, we find that:

$$K_3 = \frac{n_i^2}{N_a}\left[\exp\left(\frac{V}{U_T}\right) - 1\right] \tag{27}$$

The functions $h_k(r)$ are given by:

$$h_k(r) = X_k I_0\left(\frac{r}{L_{nk}}\right) + P_k \tag{28}$$

where: $$\frac{1}{L_{nk}^2} = \frac{1}{L_n^2} + C_k^2 \tag{29}$$

$$P_k = -2K_3\left(\frac{L_{nk}^2}{L_n}\right)^2 \frac{\sin(C_k W_b)}{\sin(C_k W_b) \times \cos(C_k W_b) - C_k W_b} \tag{30}$$

$$X_k = -\frac{P_k}{I_0\left(\frac{R}{L_{nk}}\right) + \frac{2D_n}{V_g L_{nk}} I_0'\left(\frac{R}{L_{nk}}\right)} \tag{31}$$

The dark current density in the base region is obtained from:

$$J_0^B = \frac{1}{\pi R^2}\int_0^R q D_n \left.\frac{\partial \Delta n(r,z)}{\partial z}\right|_{z=W_e + W} (2\pi r\, dr) \tag{32}$$

2.1.5 Dark current density in the emitter region:

Similarly to the base region, the boundary conditions {Eq. (14)} and {Eq. (5)} used for the emitter region in the case of an illuminated cell are also valid under dark conditions. However, {Eq. (13)} has to be replaced by the Boltzmann condition:

$$\Delta p(r, z=W_e) = \frac{n_i^2}{N_d}\left[\exp\left(\frac{V}{U_T}\right) - 1\right] \tag{33}$$

The excess minority carrier density $\Delta p(r,z)$ can be written as follows:

$$\Delta p(r, z) = \sum_{k\geq 0} h_k'(r)\sin\left[C_k' \times z\right] + K_4 \tag{34}$$

K_4 is given by the boundary condition {Eq. (33)}, we find that:

$$K_4 = \frac{n_i^2}{N_d}\left[\exp\left(\frac{qV}{KT}\right) - 1\right] \tag{35}$$

The functions $h_k'(r)$ can be written as:

$$h_k'(r) = Y_k I_0\left(\frac{r}{L_{pk}}\right) + Q_k \tag{36}$$

where: $$\frac{1}{L_{pk}^2} = \frac{1}{L_p^2} + C_k'^2 \tag{37}$$

$$Q_k = -2K_4\left(\frac{L_{pk}^2}{L_p}\right)^2 \frac{\sin(C_k' W_e)}{\sin(C_k' W_e)\times\cos(C_k' W_e) - C_k' W_e} \tag{38}$$

$$Y_k = -\frac{Q_k}{I_0\left(\frac{R}{L_{pk}}\right) + \frac{2D_p}{V_g L_{pk}} I_0'\left(\frac{R}{L_{pk}}\right)} \tag{39}$$

The dark current density in the emitter region is then given by:

$$J_0^E = \frac{1}{\pi R^2}\int_0^R q D_p \left.\frac{\partial \Delta p(r, z)}{\partial z}\right|_{z=0} (2\pi r\, dr) \tag{40}$$

So, the reverse saturation current density of the emitter-base junction is given by:

$$J_{0d} = J_0^B + J_0^E \tag{41}$$

2.2 Solar cell with multi-cylindrical grains

We propose in this section, a generalization of our model in the case of a solar cell formed by $(n\times n)$ identical cylindrical grains. When the grains are in contact, grains of complicated geometry appear (Fig. 2). The modeling of this geometry is very difficult.

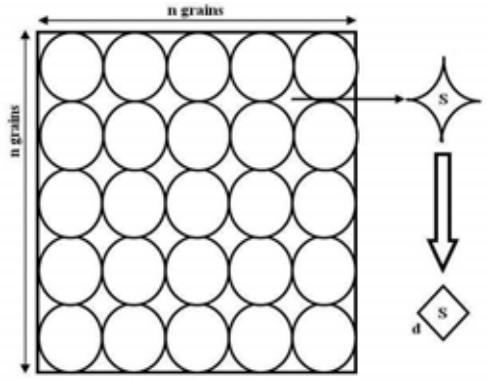

Fig. 2: Schematic presentation in the plan (x, y) of a solar cell with multi-cylindrical grains and the geometrical approach used in the calculation

An approach to the problem can be achieved by using the finite element method. However, this method requires a very accurate discretization, an important memory space and more important a very long CPU time. Thus it seems more appropriate to find a more analytical solution to the problem.

In our approach, we assimilate each grain of complicated geometry to a cubic grain having the same area ' S ', and we search the corresponding width ' d ' as a function of the cylindrical grain radius ' R ' (Fig. 2). The cubic grain number is the same as that of cylindrical grains. The contribution of the cubic grains for the photocurrent and dark current is calculated by some authors [1, 6, 15, 16].

In our case, the cubic grain area can be written as:

$$S = (4 - \pi)\, R^2 = d^2 \tag{42}$$

So that the grain width:

$$d = \sqrt{4 - \pi}\ .\ R \tag{43}$$

The intragrain boundaries are characterized by a recombination velocity equal to $V_g / 2$; but only the outer grains have a recombination velocity equal to V_g; that is the first and the last grains in the x and y directions. Consequently, the current densities:

$$J_{ph1} = J_{phn} = J_{phx} \tag{44}$$

$$J_{01} = J_{0n} = J_{0x} \tag{45}$$

The current density J_{phx} and J_{0x} have the same expressions as J_{ph} and J_0 respectively for the case of a single grain cell {Eq (24) and (41)}. But in the expressions of J_{phx} and J_{0x}, we have to replace $V_g / 2$ by V_g in the case of the cubic and cylindrical grains.

So the total current densities are given by:

$$J_{phT} = J_{phT}^{Cy1} + J_{phT}^{Cub} \tag{46}$$

$$J_{0T} = J_{0T}^{Cy1} + J_{0T}^{Cub} \tag{47}$$

Where $J_{phT}^{Cyl}\ .\ (J_{phT}^{Cub})$ and $J_{0T}^{Cyl}\ .\ (J_{0T}^{Cub})$ are the photocurrent and the dark current densities of the $(n \times n)$ cylindrical (cubic) grains.

These current densities have the following expressions:

$$J_{phT}^{Cy1} = \frac{4(n-1)\times J_{phx}^{Cy1} + \left\lfloor n^2 - 4(n-1)\right\rfloor \times J_{ph}^{Cyl}}{n^2} \tag{48}$$

$$J_{0T}^{Cy1} = \frac{4(n-1)\times J_{0x}^{Cy1} + \left\lfloor n^2 - 4(n-1)\right\rfloor \times J_{0}^{Cyl}}{n^2} \tag{49}$$

$$J_{phT}^{Cub} = \frac{4(n-1)\times J_{phx}^{Cub} + \left\lfloor n^2 - 4(n-1)\right\rfloor \times J_{ph}^{Cub}}{n^2} \tag{50}$$

$$J_{0T}^{Cub} = \frac{4(n-1)\times J_{0x}^{Cub} + \left[n^2 - 4(n-1)\right]\times J_0^{Cub}}{n^2} \quad (51)$$

2.3. Current-voltage characteristic and photovoltaic parameters

The $J-V$ characteristics of solar cell in the real case are expressed by the equivalent following equation:

$$J = J_{ph} - J_{0d}\left\{\exp\left(\frac{V+JR_S}{V_T}\right)-1\right\} - J_{0R}\left\{\exp\left(\frac{V+JR_S}{2V_T}\right)-1\right\} - \frac{V+JR_S}{R_{sh}} \quad (52)$$

with J_{ph} and J_{0d} are given by {Eq. (24)} and {Eq. (41)} respectively.

J_{0R} is the dark saturation current in the depletion region at the N^+/P junction [17].

The open circuit voltage V_{oc} is given by the resolution of the {Eq. (52)} when $J = 0$.

The power output that can be obtained from the cell is given by:

$$P = J \times V \quad (53)$$

At power maximum, $\frac{dP}{dV} = 0$ and $V = V_m$; J_m is determined since the {Eq. (52)}.

The conversion efficiency of an elementary cell is easily computed by:

$$\eta = \frac{V_m \times J_m}{P_{in}} \quad (54)$$

Where P_{in} the incident power for 1 sun AM1 (P_{in} = 0.1 W.cm^{-2}).

3. RESULTS AND DISCUSSION

3.1 Effect of the cell thickness and the grain radius on the emitter-base reverse saturation current density

The reverse saturation current density J_{od} of an N^+/P polysilicon solar cell with an elementary cylindrical grain given by {Eq. (41)} is plotted against the cell thickness H and the grain radius R in figures 3-a and 3-b.

From figure 3-a, it may be noted that, for a thin solar cell ($H > L_n$), the recombination velocity at the grain boundaries V_g has practically no effect on the reverse saturation current density especially for a passivated back surface.

Figure 3-b shows that the reverse saturation current density is very sensitive to the grain radius R especially for unpassivated grain boundaries.

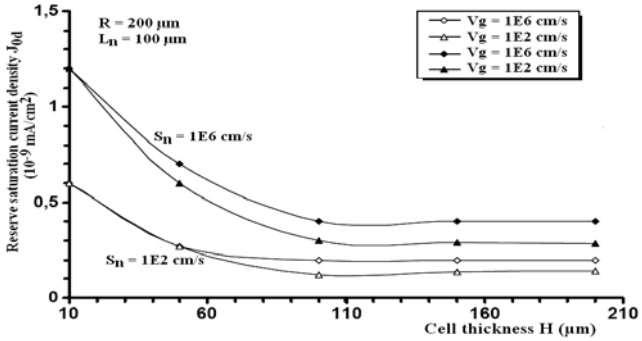

Fig. 3.a: Effect of the recombination velocity at the grain boundaries V_g on the variation of reverse saturation current density with respect to the grain thickness H for two values of S_n

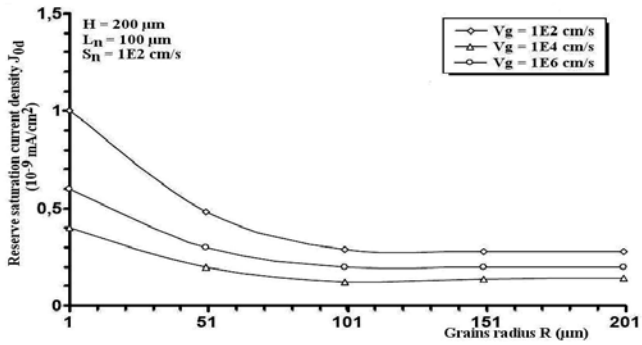

Fig. 3-b: Effect of the recombination velocity at the grain boundaries V_g on the variation of reverse saturation current density with respect to the grain radius R

3.2 Effect of the cell thickness and the grain radius on the photovoltaic parameters

Figure 4-a shows the variation of the short-circuit current density versus the cell thickness H for different values of the recombination velocity at the back contact S_n and at the grain boundaries V_g .

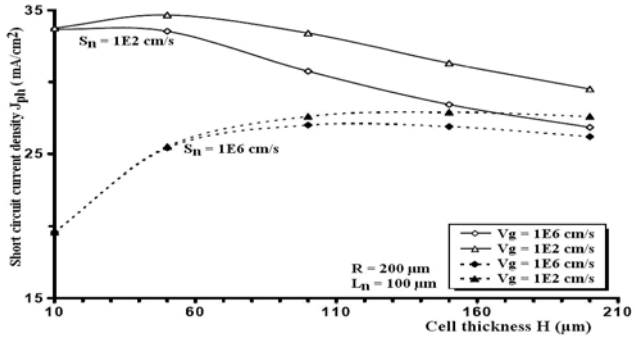

Fig. 4-a: Effect of the recombination velocity at the grain boundaries V_g on the variation of short circuit current density with respect to the grain thickness H for two values of S_n

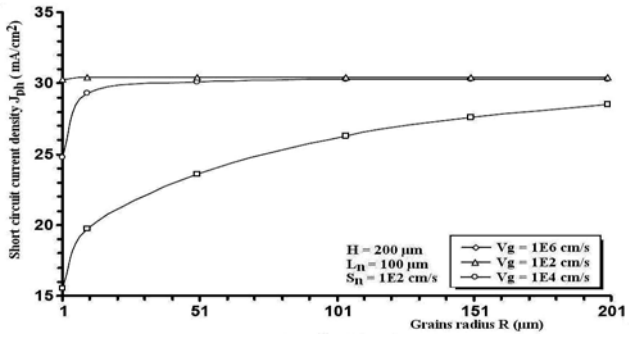

Fig. 4-b: Effect of the recombination velocity at the grain boundaries V_g on the variation of short circuit current density with respect to the grain radius R

It can be noted that, for a thin solar cell ($H < L_n$), the photocurrent depends strongly on the state of the back surface and it is insensitive to the traps states at the grain boundaries especially for unpassivated back surface. However, the recombination at the grain boundaries becomes not negligible and the photocurrent decreases for a thick solar cell ($H > L_n$) and a low cylindrical grain radius R as it is indicated in figure 4-b.

In addition the results shown in figure 4-a are in good agreement with those calculated numerically by Lanza *et al.* [10] and by Elnahwy *et al.* [12] and confirm their conclusion that the necessary cell thickness to obtain more than 95 % of the available current density is about 50 µm.

In Figure 5-a, given the variation of the open circuit voltage V_{oc} with respect to the cell thickness H for different recombination velocities at the back contact and at the grain boundaries, we can noted that the passivation of the back surface can be very interest for the enhancement of the open circuit voltage of the solar cell especially for a thin cell. This enhancement is explained by the decrease of the reverse saturation current density J_{od} given in figure 3-a.

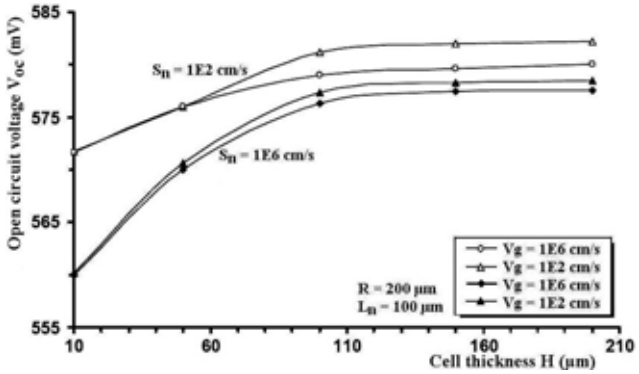

Fig. 5-a: Effect the recombination velocity at the grain boundaries V_g on the variation of the open circuit voltage with respect to the cell thickness H for different values of S_n

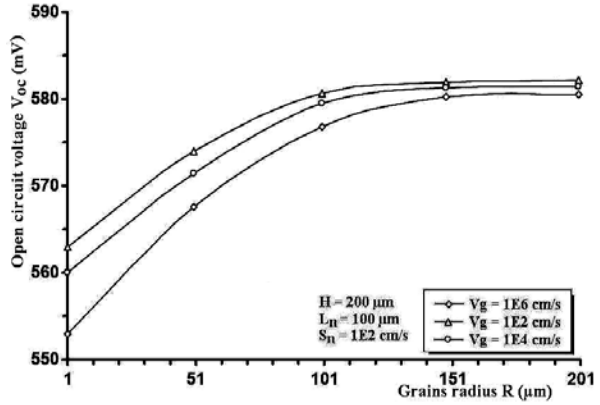

Fig. 5-b: Effect of the grain radius R on the open circuit voltage for different values of V_g

In addition, the passivation of the grain boundaries have practically no effect on the V_{oc} values especially for a thin solar cell (Fig 5-a) and for a high grain radius (Fig 5-b).

The solar cell efficiency calculated from {Eq. (54)} is plotted against the cell thickness and the grain radius as it is shown in figures 6-a and 6-b. In Fig 6-a, it can be seen that, when the back surface is well passivated, a thin solar cell is sufficient to obtain a maximal efficiency. In fact, the efficiency of a passivated solar cell can reach 14,5 % when the cell thickness is less than 50µm. Thus, the necessary cell thickness to obtain more than 95 % of the available solar cell efficiency is about 50µm.

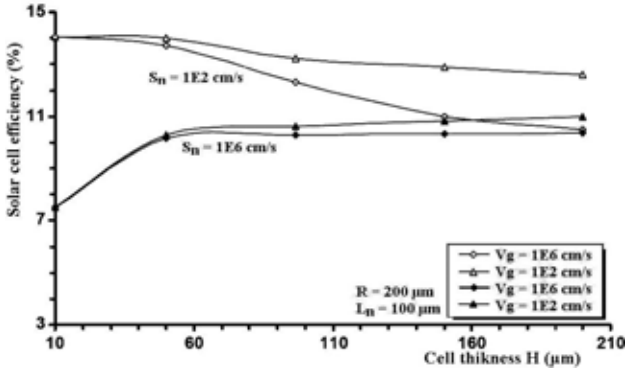

Fig. 6-a: Effect the recombination velocity at the grain boundaries V_g on the variation of the solar efficiency with respect to the cell thickness H for different values of S_n

In addition, Fig 6-b gives a comparison between our numerical model and the two-dimensional simulated one given by kurobe *et al.* [12] and interested to the polysilicon thin-film solar cell. We notice that the cell efficiency is insensitive to the grain radius especially for a passivated back surface. We confirm the conclusion given by kurobe *et*

al., that the recombination velocity at the back contact should be less than 10^3 cm/s in order to keep the efficiency as a constant regardless of the grain radius.

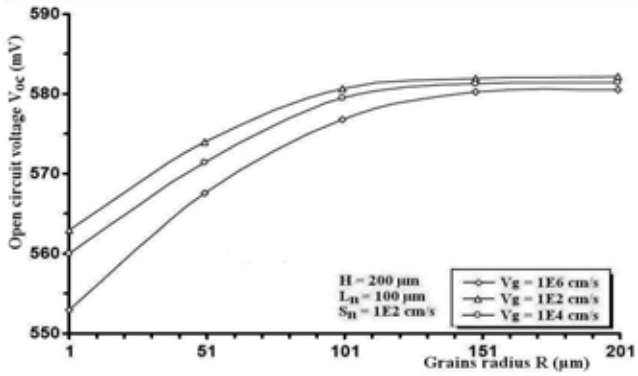

Fig. 6-b: Effect of the grain radius R on the solar cell efficiency for different values of V_g

3.3 Effect of the grain number on the parameters of polysilicon solar cell with multi-cylindrical grains

Figures 7, 8, 9 and 10 show the variations of the reverse saturation current density J_{0d}, the photocurrent density J_{ph}, the open circuit voltage V_{oc} and the solar cell efficiency with respect to the grain number for different thickness H of a solar cell formed by $(n \times n)$ identical grains.

Figure 7 shows that the reverse saturation current density J_{0d} starts insensitive to the grain number, but it becomes very sensitive to a large grain number, due to the recombination at the grain boundaries. In addition, the cell thickness H has an important effect for a small grain number when the recombination at the back surface dominates the recombination at the grain boundaries.

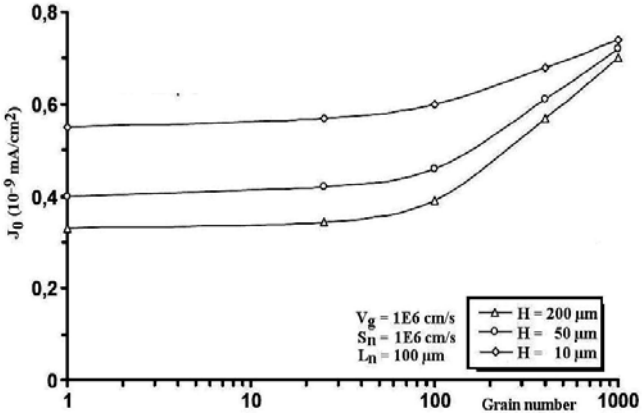

Fig. 7: Effect of the grain number on the reverse saturation current density for different values of H

In Figure 8, we notice that the photocurrent density J_{ph} decreases with the grain number especially for a thick solar cell. This decrease is due to the increase of the grain boundaries number in the cell and of the traps states at the grain boundaries. In addition, the effect of the cell thickness is important for a cell with a small grain number due to the recombination at the back contact.

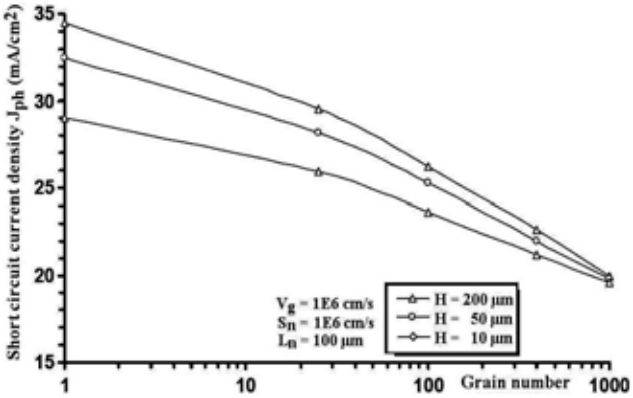

Fig. 8: Effect of the grain number on the photocurrent density for different values of H

In addition, Figure 9 shows that the open circuit voltage V_{oc} can reach 580 mV for a thick solar cell with a small grain number. But V_{oc} decreases for a large the grain number due to the effect of the grain number in the reverse saturation current density J_{od}.

In Figure 10, we can note that the efficiency can overtakes 12.5 % for a thick solar cell with a small grain number. However, for a thin solar cell, when the recombination at the grain boundaries becomes important by increasing the grain boundaries number, this parameter decreases less than 8 %. This decrease is due to the importance of the recombination at the back contact and at the grain boundaries.

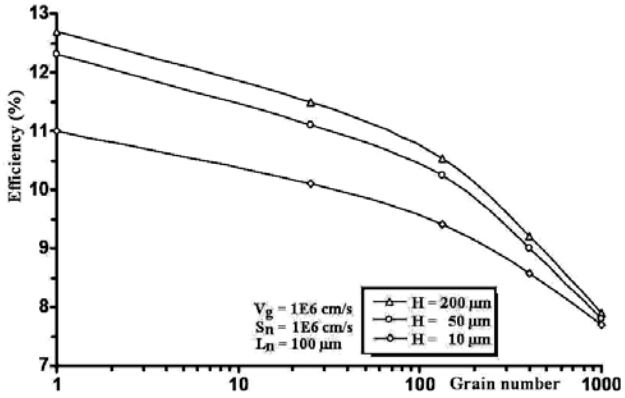

Fig. 10: Effect of the grain number on the solar cell efficiency for different values of H

So, we can say that the solar cell parameters are very sensitive to the grain number. In fact, these parameters decrease with the grain number. When the grain number is small, the polycrystalline solar cell structure approaches the crystalline cell. A small number of grain boundaries leads to a weak recombination. However, when the grain number is important, the intra-grains recombination can be significant, thus, the decrease of the photovoltaic parameters can be important especially for a thick solar cell.

4. COMPARISON BETWEEN THE CYLINDRICAL AND THE CUBIC MODELS

In this section, we suggest a comparison between the contribution of an elementary cylindrical grain solar cell and an elementary cubic grain one, having the same area on the photovoltaic parameters. The numerical results regarding the cubic grain are taken from the references [1, 6, 16, 17]. On the other hand, we compared the contribution of a solar cell formed by multi-cylindrical grains with a solar cell having the same dimensions but formed by multi-cubic grains.

Table 2 shows the short circuit current density J_{cc}, the open circuit voltage V_{oc} and the solar cell efficiency η of a cylindrical and a cubic grain as function of the grain area. We can see an improvement of the solar cell parameters for the cylindrical grain compared to those for the cubic one having the same area, due to the smaller grain boundary area in the cylindrical grain. This improvement overtakes 5,9 % in the open circuit voltage and 2,2 % in the efficiency.

Table 2: Variation of the solar cell parameters as function of the grain area in the cases of elementary cylindrical and cubic grain

Grains area (μm^2)	**50×50**	**100×100**	**150×150**	**200×200**
J_{cc} cylindrical (mA/cm^{-2})	28,1	28,72	28,96	29,1
J_{cc} cubic (mA/cm^{-2})	27,8	28,34	28,7	29
V_{oc} cylindrical (mV)	569,2	574,6	575,8	576,3
V_{oc} cubic (mV)	537,43	555,11	562,8	568,45
η cylindrical (%)	10,03	10,83	10,92	10,98
η cubic (%)	9,81	10,72	10,84	10,95

Table 3 gives the photovoltaic parameters of a solar cell formed by $(n \times n)$ cylindrical grains as function of the grain number, compared to a solar cell having the same grain number but with a cubic geometry. It is clear that the photovoltaic parameters of a multi-cylindrical grains solar cell are comparable to those of multi-cubic grains ones.

Table 3: Variation of the solar cell parameters as function of the grain number in the cases of multi-cylindrical and multi-cubic grain

Grains number $(n \times n)$	**1×1**	**5×5**	**10×10**	**20×20**
J_{cc} cylindrical (mA/cm^{-2})	34,1	31,2	27,9	22,46
J_{cc} cubic (mA/cm^{-2})	33,9	30,8	27.2	21.6

V_{oc} cylindrical (mV)	594,2	589,2	579,7	565,1
V_{oc} cubic (mV)	589,43	581,52	571,7	556,9
η cylindrical (%)	13,59	12,18	11,12	10,24
η cubic (%)	13,52	12,08	10,98	10,01

Moreover, for the solar cell with multi-cylindrical grains, we can see a small increase of the short circuit current density, the open circuit voltage and the cell efficiency, explained by the fact that the assumed quadratic grains have a smaller grain boundary area as compared to the actual grains.

5. CONCLUSION

In this paper, we have developed a three-dimensional model for a typical solar cell having the shape of a columnar cylinder. This model has permitted us to study the influence of the grain size, the recombination velocity at back contact and at the grain boundary on the photovoltaic parameters.

The results show, for a thick solar cell, that the recombination velocity at the grain boundaries has practically no effect on the photovoltaic parameters especially for a cell with a high grain radius and a passivated back surface. These results are in good agreement with those presented by Elnahwy *et al.* and Lanza *et al.*

On the other hand, we have extended the model to the case of a polycrystalline solar cell with multi-cylindrical grains. In our approach, we have assimilated the grains - with complicated geometry, appearing when the cylindrical grains are in contact - to cubic grains with the same area. We have expressed the width of the cubic grain as a function of the cylindrical grain radius. The results show a decrease of the solar cell parameters when the grain number increases especially for a thick solar cell.

Moreover, the comparison between the solar cell parameters for the elementary cylindrical grain compared to those for an elementary cubic one having the same area shows an improvement of the cylindrical cell parameters, due to the smaller grain boundary area. This improvement can reach 5.9 % in the open circuit voltage and 2.2 % in the efficiency.

In addition, in comparison between multi-cubic and multi-cylindrical grains solar cell having the same grain number, we noted a small increase of the short circuit current density, the open circuit voltage and the cell efficiency.

This study can be extended by introducing the influence of the grain boundaries' orientation on the solar cell parameters.

NOMENCLATURE

$\Delta n(r,z)$: Density of excess minority carrier (electrons) in the base

$\Delta p(r,z)$: Density of excess minority carrier (holes) in the emitter

L_n : Diffusion length of minority carrier in the base

L_p : Diffusion length of minority carrier in the emitter

D_n : Diffusion constant of minority carrier in the base

D_p : Diffusion constant of minority carrier in the emitter

W_e : Thickness of the emitter region

W : Width of the depletion region

W_b : Thickness of the base region

H : Total cell thickness

S_n : Recombination velocity at the back contact

V_g Recombination velocity at the grain boundaries

S_p : Surface recombination velocity

J_{ph} : Total photogenerated current density

C_k : Eigenvalues for the eigenfunction used for the “r” direction

$\alpha(\lambda)$: Coefficient of absorption of silicon at a wavelength λ

J_{ph}^{B} Photogenerated current density in the base

J_{ph}^{E} Photogenerated current density in the emitter

J_{ph}^{R} : Photogenerated current density in the depletion region

N_a : Doping concentration in the base

N_d : Doping concentration in the top region

n_i : Intrinsic carrier concentration

V : Applied voltage

U_T : Thermal voltage

J_0^B : Dark current density in the base

J_0^E : Dark current density in the emitter

J_{0R} : Dark current density in the depletion region

REFERENCES

[1] S.N. Mohammad and C.E. Rogers, ‘*Current-Voltage Characteristics and Performance Efficiency of Polysilicon Solar Cells*’, Journal of Solid-State Electronics, Vol. 31, N°8, pp. 1221 - 1228, 1988.

[2] J. Dugas, ‘*Modelling of Material Properties Influence on Back Junction Thin Polycrystalline Silicon Solar Cells*’, Solar Energy Materials and Solar Cells, Vol.43, N°2, pp 193 - 202, 1996.

[3] A. Rohatgi and P. Rai houdhury, ‘*Design, Fabrication and Analysis of 17-18 % Efficient Surface Passivated Silicon Solar Cells*’, IEEE Transactions on Electron Devices, Vol. ED-31, N°5, pp. 596 - 601, 1984.

[4] S. Elnahwy and N. Adeeb, ‘*Thin Film Polycrystalline Si p-n Junction Solar Cells with Preferential Doping*’, Journal of Solid-States Electronics Vol. 25, N°11, pp. 1111 – 1117, 1982.

[5] A.K. Ghosh, C. Fishman and T. Feng, ‘*Theory of the Electrical and Photovoltaic Properties of Polycrystalline Silicon*’, Journal of Applied Physics, Vol. 51, N°1, pp. 446 - 454, 1980.

[6] S.N. Mohammad, Journal of Applied Physics, Vol. 58, p. 751, (1985).

[7] A. Ben Arab, N. Fourati and N. Lakhoua, ‘*Preferential Doping Contribution to the Photoresponse of Polysilicon Solar Cells*’, Solar Cells, Vol. 29, N°1, pp. 49 - 62, 1990.

[8] B. Ba, M. Kane, A. Fickou and G. Sissoko, ‘*Excess minority carrier densities and transient short circuit currents in polycrystalline silicon solar cells*’, Solar Energy Materials and Solar Cells, Vol. 31, N°1, pp. 33 - 49, 1993.

[9] K-I. Kurobe, Y. Ishikawa, Y. Yamamoto, T. Fuyuki and H. Matsunami, ‘*Effects of Grain Boundaries in Polycrystalline Silicon Thin-Film Solar Cells Based on the Two-Dimensional Model*’, Solar Energy Materials and Solar Cells, Vol. 65, N°1-4, pp. 201 - 209, 2001.

[10] C. Lanza and H.J. Hovel, ‘*Efficiency Calculations for Thin-Film Polycrystalline Semiconductors Schottky Barrier Solar Cells*’, IEEE Transactions on Electron Device, Vol. ED-24, p. 392 - 396, 1977.

[11] C. Lanza and H.J. Hovel, '*Efficiency Calculations for Thin-Film Polycrystalline Semiconductor p-n Junction solar Cells*', IEEE Transactions on Electron Device, Vol. 27, N°11, pp. 2085 - 2088, 1980.

[12] S. Elnahwy and N. Adeeb, '*Exact Analysis of a Three-Dimensional Cylindric Model for a Polycrystalline Solar Cell*', Journal of Applied Physics, Vol. 64, N°10, pp. 5214 - 5319, 1988.

[13] M. Ben Amar, Revue Internationale d'Héliotechnique, Vol. 3, p. 24, 2001.

[14] A. Ben Arab, '*An Accurate Solution for the Dark Diffusion Current of Preferentially Doped Polysilicon Solar Cells*', Journal of Solid-State Electronics, Vol. 37, N°7, pp. 1395 - 1401, 1994.

[15] S.M. Sze, '*Physics of Semiconductors Devices*', Bell Labotories Inc., Murray Hill New-Jersey, 1991.

[16] S. Elnahwy and N. Adeeb, '*Analysis of the effect of a Uniform Base Drift Field on the Performance of a Polycrystalline p//n Junction Solar Cells*', Journal of Solid-States Electronics, Vol. 33, N°2, pp. 169 - 176, 1990.

[17] J. Dugas and J. Oualid, '*A Model of the Dependence of Photovoltaic Properties on Effective Diffusion Length in Polycrystalline Silicon*', Solar Cells, Vol. 20, N°3, pp. 167 - 176, 1987.